Hindawi Publishing Corporation
Journal of Nanomaterials
Volume 2007, Article ID 80814, 8 pages
doi:10.1155/2007/80814

Research Article

3D-Simulation of Topology-Induced Changes of Effective Permeability and Permittivity in Composite Materials

B. Hallouet and R. Pelster

Fachrichtung 7.2, Experimentalphysik, Universität des Saarlandes, Postfach 151150, 66041 Saarbrücken, Germany

Received 15 February 2007; Revised 11 May 2007; Accepted 4 June 2007

Recommended by Christian Brosseau

We have performed 3D simulations of complex effective permittivity and permeability for random binary mixtures of cubic particles below the percolation threshold. We compare two topological classes that correspond to different spatial particle arrangements: cermet topology and aggregate topology. At a low filling factor of $f = 10\%$, where most particles are surrounded by matrix material, the respective effective material parameters are indistinguishable. At higher concentrations, a systematic difference emerges: cermet topology is characterized by lower effective permittivity and permeability values. A distinction between topological classes might thus be a useful concept for the analysis of real systems, especially in cases where no exact effective-medium model is available.

1. INTRODUCTION

Composite materials have a lot of technical applications, and especially magnetic nanocomposites have been studied recently [1–3]. The fundamental question is how the properties of their components and their microstructure contribute to the effective properties of the new material. Besides a multiplicity of approximative mixture formulas, there are some analytical solutions of the so-called effective-medium problem (see, e.g., [4–8]). Also 2D and 3D computer simulations allow to predict the effective material parameters for various particle arrangements and shape (see, e.g., [9–17]). The inherent structure-dependence is beyond controversy and in the strict sense every microstructure can give rise to a different mixture rule. Therefore, the analysis of nanocomposites, for example, of nanoparticles dispersed in a host material, represents a challenge: due to the difficulty to control a spatial particle arrangement on a nm scale, the exact microstructure is often unknown. Nevertheless, we are still interested either in predicting the properties of the composite or in studying the dispersed nanoparticles that do not necessarily behave like bulk material (the latter case represents the so-called inverse problem, where measured effective quantities are used to evaluate the properties of a component). For both cases, at least approximative procedures are required. In view of this fact, we raise a fundamental question regarding the concept of topological classes. More precisely, we want to find out to what extend it is useful to distinguish between two topological classes.

In the following, we consider composite materials consisting of 2 phases that we call "matrix" and "particles" (indices "m" and "p"). In order to attribute an effective permittivity and an effective permeability to these mixtures, the structural inhomogeneities have to be sufficiently small compared to the wavelength of an applied electromagnetic field. According to their definition as volume averaged quantities [18, 19], the effective material parameters are independent of the size of the inclusions, but depend on the volume filling factor of the particles $f = V_p/V_{\text{total}}$ as well as on the properties of the two components,

$$\frac{\varepsilon_{\text{eff}}}{\varepsilon_m} = \mathcal{F}\left(f, \frac{\varepsilon_p}{\varepsilon_m}\right), \tag{1}$$

whereas the function $\mathcal{F}$ depends on the microstructure. The same holds for the magnetic permeability, presupposed that the field excitation is unchanged (consider, e.g., a sample in a homogeneous electric or magnetic field):

$$\frac{\mu_{\text{eff}}}{\mu_m} = \mathcal{F}\left(f, \frac{\mu_p}{\mu_m}\right). \tag{2}$$

According to a formalism developed by Bergman, Fuchs, and Milton, it is even possible to separate the influence of

microstructure, characterized by a spectral density function g, from that of the components, characterized by their material parameters [20]: the effective permittivity can be written as

$$\frac{\varepsilon_{\text{eff}}}{\varepsilon_m} = 1 + f\left\{\frac{C}{t} + \int_0^1 \frac{g_f(n)}{t+n}dn\right\} \tag{3}$$

with $t = 1/(\varepsilon_p/\varepsilon_m - 1)$ and C being the strength of percolation describing the contribution of infinite clusters. Although there is no method to determine $g_f(n)$ from first principles, the theoretical consequences are quite clear: every new microstructure requires a new calculation of the effective properties. The implications for the analysis of real systems are not so explicit. Do experimental physicists need a different mixture formula for every real sample system? And how should they select one when no detailed information about the microstructure is available? In such cases, where it is impossible to choose an "exact" model, topological criteria are applied to find the best approximation for the system under study.

Generally, two topological classes are considered in the description of binary composite materials [18]. On the one hand the so-called matrix inclusion topology (cermet topology, separated grain structure), where a discontinuous phase (e.g., particles below the percolation threshold f_c) is dispersed in a continuous host matrix, all regions of which are perfectly interconnected (e.g., a polymer or a liquid, see Figures 1(a) or 3(a)). Here matrix and filler are not topologically equivalent. For example, an exact analytical solution for an arbitrary spatial configuration of well-separated spheres has been formulated in [6]. Based on this, 3D computer simulations were performed [21] showing that two of the well-known effective medium formulas for randomly dispersed particles describe the limits of very narrow and very broad particle-size distributions (see Figure 2): for monodisperse spheres Maxwell-Garnet formula holds:

$$\varepsilon_{\text{eff}} = \varepsilon_m \cdot \left(1 + f \cdot \frac{\varepsilon_p - \varepsilon_m}{\varepsilon_m + (1-f)\cdot 1/3 \cdot (\varepsilon_p - \varepsilon_m)}\right), \tag{4}$$

while for polydisperse systems with a sufficiently broad size-distribution the Hanai-Bruggeman formula applies:

$$\left(\frac{\varepsilon_{\text{eff}} - \varepsilon_p}{\varepsilon_m - \varepsilon_p}\right) \cdot \left(\frac{\varepsilon_m}{\varepsilon_{\text{eff}}}\right)^{1/3} = (1-f). \tag{5}$$

The latter is often successfully applied to describe experimental data, since most real systems are polydisperse (see, e.g., [22]). But of course, depending on the degree of agglomeration, real systems can show more complicated nonrandom spatial arrangements so that the above mixture rules are no longer valid (see, e.g., [23]).

On the other hand, there is the so-called aggregate topology, where both phases are topologically equivalent (see Figures 1(b) or 3(b)). This equivalence reflects in the symmetry of the corresponding mixture formula: interchanging both phases, $\varepsilon_p \leftrightarrow \varepsilon_m$ and $f \leftrightarrow (1-f)$, does not affect the result: $\varepsilon_{\text{eff}}(\varepsilon_p, \varepsilon_m, f) = \varepsilon_{\text{eff}}(\varepsilon_m, \varepsilon_p, 1-f)$. An example is, for example,

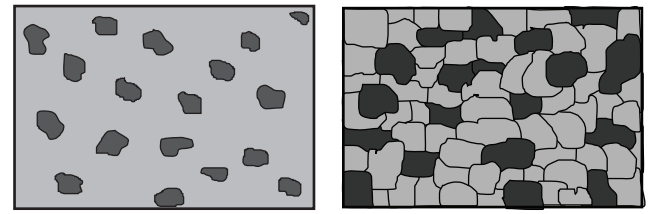

(a) (b)

Figure 1: (a) Matrix inclusion topology (cermet topology, separated grain structure) describing discrete particles that are dispersed in a continuous host phase. (b) Aggregate topology, where two topologically equivalent phases are mixed (compact powders consisting of two types of particles, polymer mixtures, interpenetrating network structures, etc.) For an idealized system, see Figure 3.

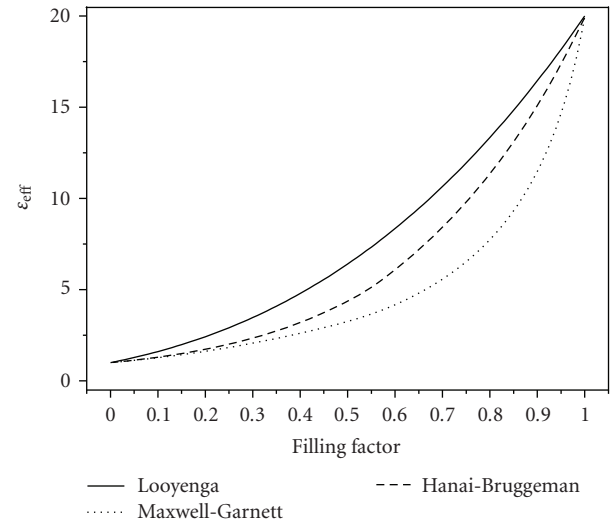

Figure 2: Effective permittivity versus volume filling factor for a binary mixture with $\varepsilon_p = 20$ and $\varepsilon_m = 1$: examples for matrix inclusion topology (model of Maxwell-Garnett, (4), and Hanai-Bruggeman, (5)) and aggregate topology (model of Looyenga, (6)).

the formula of Landau, Lifshitz, and Looyenga (see Figure 2)

$$\varepsilon_{\text{eff}}^{1/3} = f\varepsilon_{\text{eff}}^{1/3} + (1-f)\varepsilon_m^{1/3}. \tag{6}$$

The aggregate topology is, for example, appropriate for compact powders, heterogeneous polymer mixtures, and interpenetrating network structures [19]. In a range of filling factors, where both phases are above their percolation threshold, they exhibit a high degree of interconnection and form some kind of interwoven network. In this case, even particles in a continuous host phase can be approximated fairly well by the aggregate topology. For example, in a recent study, experimental data for granular material (pulverized samples, i.e., air-particle mixtures) was compared with 6 effective media formulas, 3 of them belonging to the cermet topology, and 3 to the aggregate topology, and the above Looyenga-equation performed best [24]. In Figure 2, we compare the above mixture formulas. The model of Looyenga yields higher effective

values, but it is not clear whether this is a fundamental feature of the aggregate topology: there is a multiplicity of approximative formulas for both topologies [25, 26], the respective range of validity is sometimes difficult to assess, and we have just made an arbitrary choice of 3 models.

Summarizing, there is some experimental evidence that depending on the concentration range, a topological discrimination might be a useful concept: above the percolation threshold formulas of the "aggregate type" perform well, while below this threshold formulas of the "cermet type" can yield good approximations (at least for systems of well separated particles). But it is difficult to asses whether this difference is of fundamental nature and whether it persists when we compare nonpercolating systems with an identical particle concentration.

In this article, we thus want to shed some light on the difference between both topologies. We focus on composite materials at filling factors below the percolation threshold, where in both cases the dispersed phase does not form a continuous network. For this purpose, we have performed computer simulations of 3D systems containing dispersed cubic particles as sketched in Figure 3. With monodisperse particles of this shape, it is possible to realize both topologies just by varying their spatial arrangement. For a given concentration, the respective microstructures look rather similar (and they would be hardly distinguishable without indicating the cubic grid in the sketch of the aggregate topology): there are just particles in a matrix. We would like to know whether, despite this similarity, the effective properties differ considerably. Only in this case the concept of topological classes might help to discriminate between effective medium models and to select the best approximation for the analysis of experimental data.

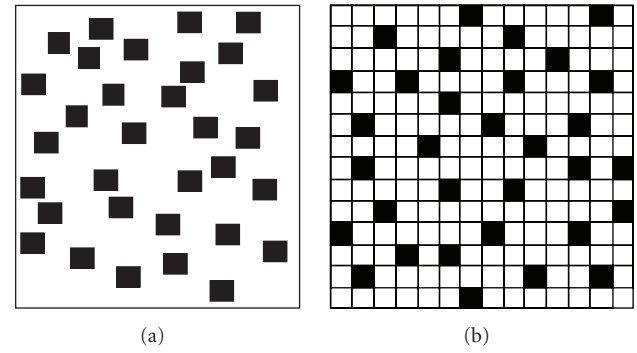

Figure 3: Sketch of an isotropic composite material containing randomly dispersed cubic particles: (a) Matrix inclusion topology, where the particle positions are arbitrary (only particle overlap is excluded). (b) Aggregate topology, where the particles are randomly dispersed on a cubic grid (a random mixture of cubes of material "p" and "m").

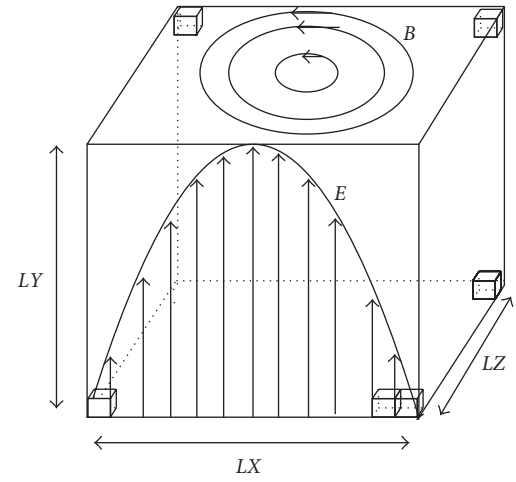

Figure 4: Distribution of electric and magnetic fields inside a resonator of size $LX * LY * LZ$ (for an empty resonator in the fundamental mode). When the resonator is filled with cubes of matrix material or particles, this leads to local changes of the field distribution and to a change of resonance frequency.

2. SIMULATION

2.1. Method

Filling a resonator with a material leads to a change of its complex resonance frequency, an effect that can be used to determine the effective material parameters of a composite:

$$\nu = \frac{\nu_0}{\sqrt{(\varepsilon\mu)_{\text{eff}}}}, \tag{7}$$

with ν_0 being the resonance frequency of the empty resonator and ν that of the material-filled resonator (these are complex frequencies, whereas the imaginary part reflects losses [27]). The simulation is based on the discretization of the Maxwell laws in such a resonator with dimensions $LX * LY * LZ$. Resonator and field distribution of the fundamental mode are sketched in Figure 4. The simulation code was developed by Stölze and Leinders [9–11], who used it to simulate an aggregate topology. It allows to calculate the complex effective permittivity ε_{eff} and permeability μ_{eff} of a 3D binary mixture in the following way.

The resonator is filled randomly with N cubes of side length a [$N = (LX/a) * (LY/a) * (LZ/a)$], either particles or matrix material, according to the respective volume fraction (see Figure 5). Such an inhomogeneous filling leads to a local pertubation of the fields compared to the well-known analytical solution for an homogeneous filling. The local distribution of electric and magnetic fields in the resonator is calculated following an approach developed by Weiland (see [9–11]). As displayed in Figure 6, a tripod of electric field is assigned at the edges of each cube forming the cubic grid G. A reciprocal grid G*, shifted by a half diagonal from the first grid G, contains the magnetic field vectors so that they penetrate the surfaces of the cube. The discretisation of the Maxwell equations on these grids leads to an eigenvalue equation that is solved via an algorithm developed by Stölze (for more information we refer to [9–11]). So the field vectors as well as the complex resonance frequency are determined. The latter information allows us to calculate the

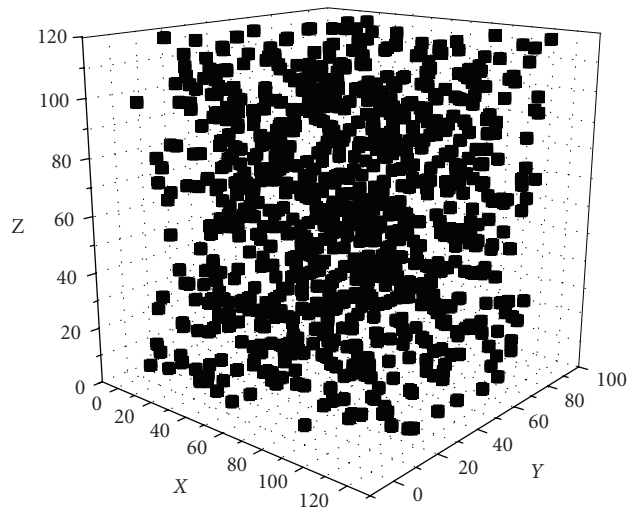

Figure 5: Spatial distribution of the particles for a filling factor of 0.56% (size of the resonator: $120a * 90a * 120a$). Different random distributions yield the same effective permittivities or permeabilities within a maximum deviation of 0.5%.

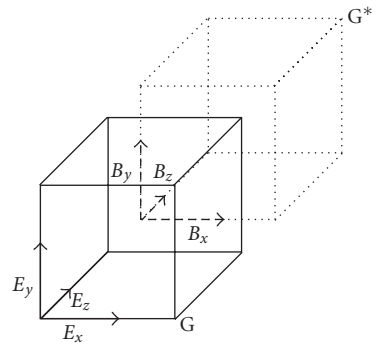

Figure 6: Representation of field vectors inside the resonator. The electric field is calculated along the first grid G (of side length a), the magnetic field along the reciprocal grid G* which is shifted by half a cube diagonal from the first grid.

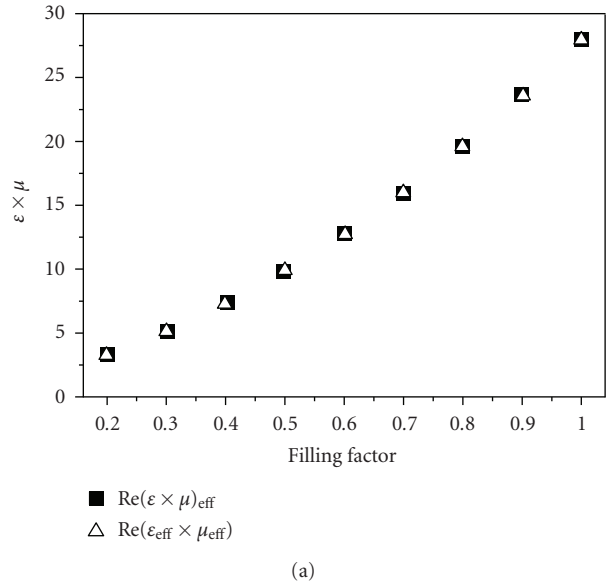

(a)

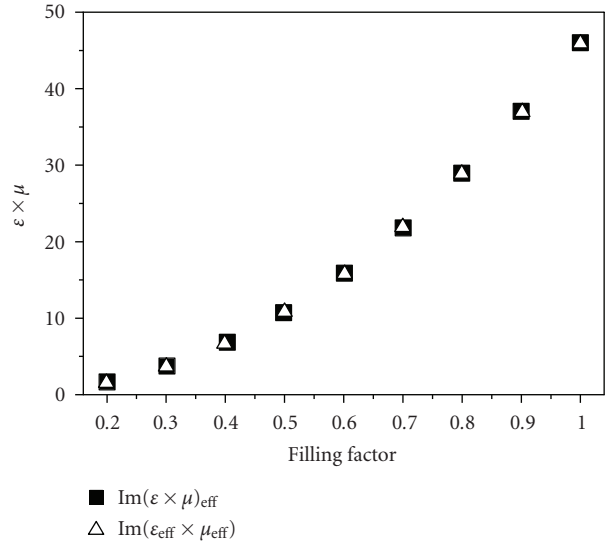

(b)

Figure 7: Real (a) and imaginary (b) parts of the product of permittivity and permeability for a binary mixture simulated in two different ways. Filled cubes: $(\varepsilon \cdot \mu)_{\mathrm{eff}}$ resulting from one simulation run with $\varepsilon_p = 10 - 4i$, $\varepsilon_m = 1$, $\mu_p = 4 - 3i$, and $\mu_m = 1$. Open triangles: $\varepsilon_{\mathrm{eff}} \cdot \mu_{\mathrm{eff}}$ calculated from two simulation runs, a dielectric one ($\varepsilon_p = 10 - 4i$, $\varepsilon_m = \mu_p = \mu_m = 1$ yielding $\varepsilon_{\mathrm{eff}}$) and a magnetic one ($\mu_p = 4 - 3i$, $\mu_m = \varepsilon_p = \varepsilon_m = 1$ yielding μ_{eff}). Obviously, $(\varepsilon \cdot \mu)_{\mathrm{eff}} = \varepsilon_{\mathrm{eff}} \cdot \mu_{\mathrm{eff}}$ holds.

product $(\varepsilon\mu)_{\mathrm{eff}}$ from the complex resonance frequencies of the empty and the filled resonator according to (7).

In order to obtain $\varepsilon_{\mathrm{eff}}$ and μ_{eff} separately, two simulation runs are necessary. In the first one, a nonmagnetic system ($\mu_p = \mu_m = 1$) is considered yielding $\varepsilon_{\mathrm{eff}}$. In the second run, μ_{eff} is evaluated for a purely magnetic material ($\varepsilon_p = \varepsilon_m = 1$). In Figure 7, we show that the product of these values, $\varepsilon_{\mathrm{eff}} \cdot \mu_{\mathrm{eff}}$, equals the value of $(\varepsilon\mu)_{\mathrm{eff}}$ that results from a single run (where $\mu_p \neq 1$ and $\varepsilon_p \neq 1$). Two final remarks are necessary.

(i) Since effective permeability and permeability are a function of $\varepsilon_p/\varepsilon_m$ and μ_p/μ_m, we can set $\varepsilon_m = \mu_m = 1$ in all simulations without loss of generality (see (1) and (2)). A high contrast between matrix and particles results in higher effective material parameters, so that structure-induced changes can be monitored more easily. In the following, we therefore choose particle parameters $|\varepsilon_p| \gg 1$ or $|\mu_p| \gg 1$.

(ii) Due to the resonator geometry, the effective permittivity is evaluated for an electric field parallel to a symmetry axis of the cubic grid ($E \parallel y$, see Figure 4), while the circumferential magnetic field yields a different volume average. For this reason, different functions $\mathcal{F}$ describe the magnetic and dielectric responses (see (1) and (2) as well as [11]).

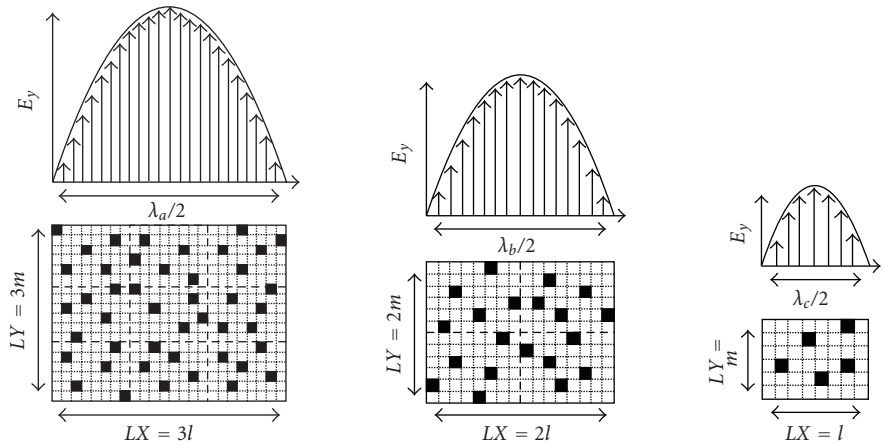

Figure 8: Testing for size effects by varying the resonators dimensions with respect to the particle size (aggregate topology).

In this work, we have used the original code of Stölzle and Leinders, that the authors kindly put at our disposal (we made only some minor technical modifications). Implemented on a modern personal computer (64- bit processor, 2.2 GHz, 4 GB RAM), it allows to simulate much bigger systems than those shown in the original work (having a size of $40a \times 30a \times 40a$ [9–11]). We are now able to simulate systems up to a size of $120a \times 90a \times 120a$ in a reasonable time [28]), that is, on average it takes several hours to calculate an effective permittivity or permeability (the evaluation of permeability requires less CPU time). As a consequence, we can study more complex systems and we are no longer restricted to the pure aggregate topology, as we shall show in the following.

2.2. Numerical test for size effects

A freely propagating wave exhibits a constant frequency, but the wavelength depends on the dielectric and magnetic properties of the medium. In a resonator, the situation is different. The wavelength is fixed and the resonance frequency changes depending on the filler medium (7). Here we consider the fundamental mode of a rectangular waveguide resonator with $LX = LZ$, so that $\lambda/2 = LX$ holds (see Figure 4). As long as the structural inhomogeneities are small compared to the wavelength, the effective material parameters of a composite depend on the microstructure but not on the absolute size d of the inclusions (1)–(3). In addition, the discretization of the resonator, that is, the grid size a, has to be sufficiently fine in order to assure a precise calculation of field distribution and resonance frequency. Therefore,

$$2 \cdot LX = \lambda_{\text{res}} \gg d, a \tag{8}$$

has to hold in order to guarantee that the effective parameters are well defined and to exclude finite size effects of the simulation.

We check this for the aggregate topology and we start with a situation where particle dimension and grid size are identical quantities, $a = d$. For this purpose, we keep $d = a$ constant and change the size of the resonator and thus the wavelength as indicated in Figure 8. We start with a maximum resonator size of $LX * LY * LZ = 120a * 90a * 120a$ and simulate the effective permeability of a binary mixture ($\mu_p = 20 - 12i$, $\mu_m = 1$, $\varepsilon_p = \varepsilon_m = 1$). This value is taken as a reference value. Then we repeat the same procedure for a two-time smaller resonator ($60a * 45a * 60a$), a three-times smaller resonator, and so on. In Figure 9, we display the relative deviation of the effective permeability as a function of the

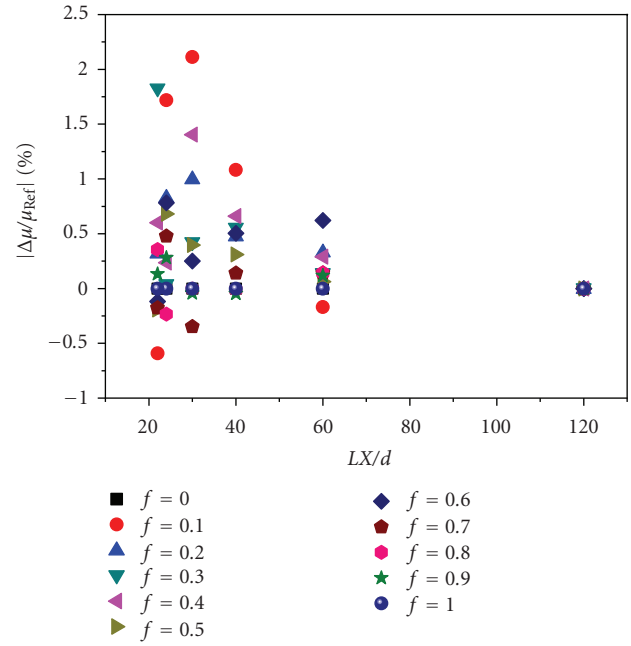

Figure 9: Variation of the absolute value of permeability as a function of system size or wavelength, $Lx/d = \lambda/(2d)$ for different filling factors $0 \le f \le 1$ (aggregate topology with $d = a$, see Figure 8). The respective effective permeability of the largest system, $LX * LY * LZ = 120a * 90a * 120a$, is taken as reference value (simulation parameters: $\mu_p = 20 - 12i$, $\mu_m = 1$, $\varepsilon_p = \varepsilon_m = 1$).

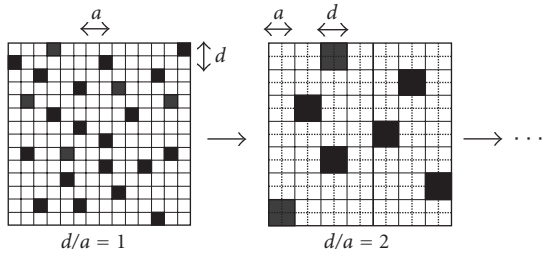

Figure 10: Testing for finite size effects by varying the ratio of particle size over grid size, d/a, while the size of the resonator is kept constant (aggregate topology). According to Figure 9 and (9) the finest discretization that can be realized corresponds to $d = 6 \cdot a$.

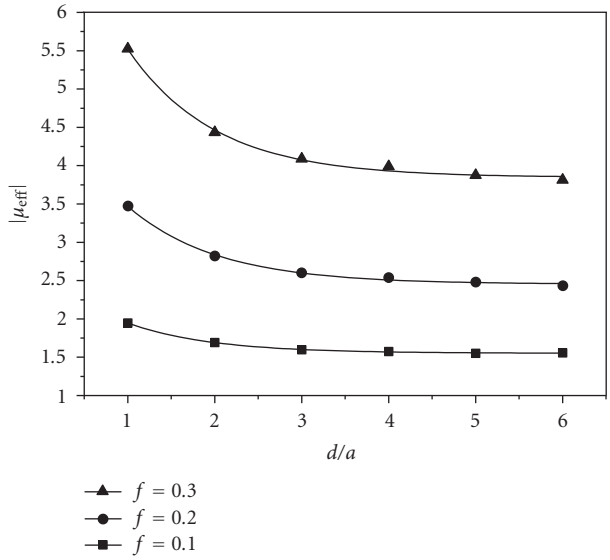

Figure 11: Variation of the absolute value of permeability as a function of the ratio of particle size to grid size for an aggregate topology (see Figure 10). The system size is approximately constant, $LX \cdot LY \cdot LZ \simeq 120a \cdot 90a \cdot 120a$. $d/a = 1$ corresponds to a coarse and $d/a = 6$ to a fine discretization of the particles (simulation parameters: $\mu_p = 20 - 12i$, $\mu_m = 1$, $\varepsilon_p = \varepsilon_m = 1$). The lines are a guide to the eyes (fit functions of the form $|\mu_{\text{eff}}| = \alpha + \beta \cdot \exp(-\gamma \cdot d/a)$). For $d/a \geq 4$, the discretization is sufficiently fine so that the calculated effective permeability reaches a saturation value.

relative resonator dimension Lx/d for filling factors between 0 and 1. The largest deviations (up to 2%) occur for small systems or big particles. Therefore, the permeability does not depend on the particle size (or at least only in a marginal way) as long as

$$\frac{LX}{d} = \frac{\lambda_{\text{res}}}{2d} \geq 20 \tag{9}$$

holds.

In the next step, we have to adjust the grid size a with respect to the particle size d in order to make sure that the electromagnetic fields inside the particles are calculated with

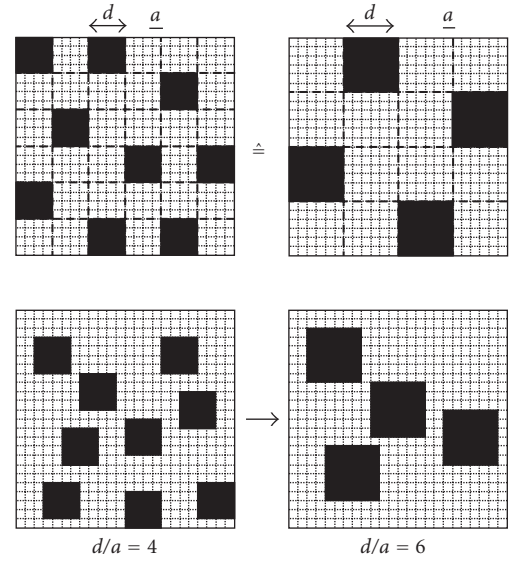

Figure 12: In order to monitor a topological transition from aggregate to cermet topology, random binary mixtures at constant volume filling factor but with different spatial particle arrangement are compared. Upper row: aggregate topology for increasing ratio of particle size d to grid size a. Lower row: intermediate topologies, where the same particles are arbitrarily dispersed on the grid. The limit $a/d \to 0$ corresponds to the cermet topology, where the particles can be located everywhere in 3D space.

a sufficiently high accuracy. For this purpose, we now keep the resonator approximately constant ($LX * LY * LZ \simeq 120a \cdot 90a \cdot 120a$) and vary the ratio d/a as indicated in Figure 10. While the electromagnetic fields are calculated on a fine grid of size a (about $1.3 \cdot 10^6$ cubic cells of size a^3), the particles are randomly distributed on a coarse grid of size $d = n \cdot a$, so that we always maintain the aggregate topology. We do this from $d/a = 1$ up to the finest discretization $d/a = 6$. This upper limit corresponds to the largest particle size that still fulfills (9). The high number of cells of size d^3 filled with material m or p guarantees a good statistics for the simulation of a random mixture. For example, at $d/a = 4$, we have more than 20 000 material cubes, at $d/a = 6$ still more than 8200. The results of the respective simulations are displayed in Figure 11. For low ratios of d/a, there is a systematic decrease of the effective permeability. For

$$d \geq 4a, \tag{10}$$

the discretization is sufficiently fine and the calculated permeability values approach a saturation value (from $d/a = 5$ to $d/a = 6$ they change by less than 2% for $f = 0.2$ and $f = 0.3$, while there is no change for $f = 0.1$). Summarizing, we are able to simulate particles with side lengths from $d = 4a$ up to $d = 6a$ without the appearance of any finite size effect and with a precision of the order of 2% (including systematic errors and repeatability of different random distributions).

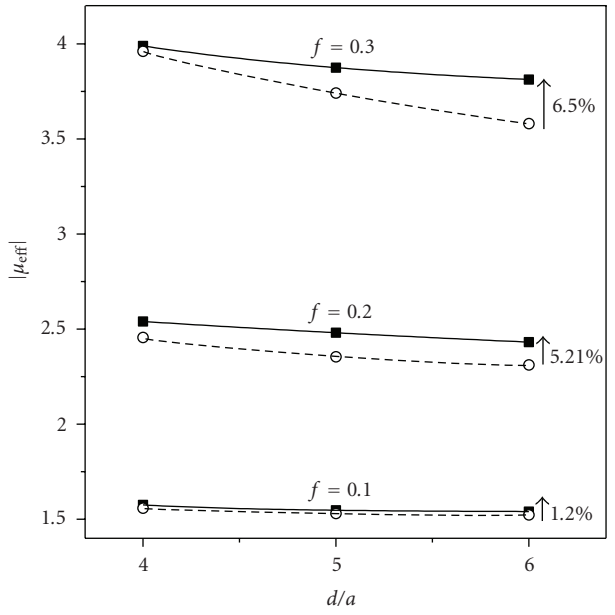

Figure 13: Absolute value of effective permeability vs ratio d/a for different volume filling factors. Filled cubes: aggregate topology. Open circles: intermediate topologies as sketched in Figure 12. Simulation parameters: $\mu_p = 20 - i \cdot 12$, $\mu_m = \varepsilon_p = \varepsilon_m = 1$. The lines are a guide to the eyes. The arrows indicate the relative differences at $d/a = 6$.

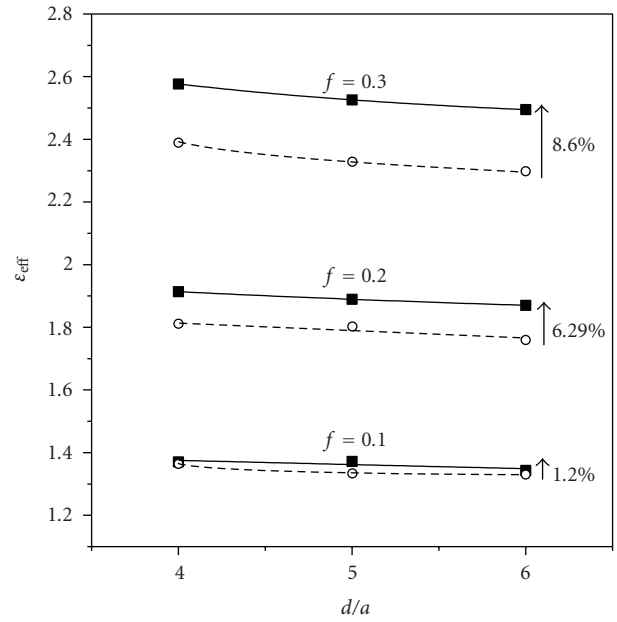

Figure 14: Effective permittivity versus ratio d/a for different volume filling factors. Filled cubes: aggregate topology. Open circles: intermediate topologies as sketched in Figure 12. Simulation parameters: $\varepsilon_p = 10$, $\varepsilon_m = \mu_p = \mu_m = 1$. The lines are a guide to the eyes. The arrows indicate the relative differences at $d/a = 6$.

3. SIMULATING A TRANSITION FROM AGGREGATE TO CERMET TOPOLOGY

Until now we have only studied the aggregate topology, simulating random binary mixtures as shown in the upper row of Figure 12. We can realize this type of microstructure for different ratios of particle size d to grid size a whereas the effective properties remain unchanged. This was simply achieved by assigning only particle positions on a coarse grid of size $d = n \cdot a$. Now we can lift this restriction so that we obtain new spatial arrangements as sketched in the lower row of Figure 12. Cubic particles of side length $d = n \cdot a$ are randomly distributed in a grid of size a. With increasing ratio of d/a, the distance between two particles can become arbitrary small in comparison with their size. The limit $a/d \to 0$ corresponds to the cermet topology sketched in Figure 3(b). Compared to the particle size d, the grid is so fine that the matrix can be considered as a continuous phase hosting the dispersed discrete particles.

The topological transition can thus be monitored as follows. We keep the volume filling factor f constant and for each ratio d/a, we compare the effective material parameters of the aggregate and of the respective intermediate topology (upper and lower rows in Figure 12). We do this for $d/a \geq 4$, where finite size effects are sufficiently small. With increasing ratio d/a, the aggregate topology remains unchanged while the intermediate topologies approach the cermet topology.

We start with a binary mixture containing magnetic particles with losses. As before we set $\mu_p = 20 - i \cdot 12$ and $\mu_m = \varepsilon_p = \varepsilon_m = 1$. Figure 13 displays the absolute value of the effective permeability as a function of d/a for particle concentrations from 10% to 30%, that is, below the percolation threshold. The aggregate topology shows the plateau values already presented in Figure 11. The behaviour of the intermediate topologies depends on the particle concentration: at low filling factor of $f = 10\%$, the results equal those for the aggregate topology (within the accuracy of the simulation). At higher concentrations systematic deviations are observed. The effective permeability values are lower by about 5% at $f = 20\%$ and by 6.5% at $f = 30\%$. Since there is only a weak dependency on d/a at $f = 10\%$ and $f = 20\%$, the simulated values can be taken as a good approximation of the cermet topology. At $f = 30\%$, however, $|\mu_{\text{eff}}|$ does not attain a plateau value, so that we can expect even smaller values for the limiting case of the cermet topology.

Next let us check how loss-free particles behave. This time we choose a purely dielectric system with $\varepsilon_p = 10$ and set $\varepsilon_m = \mu_p = \mu_m = 1$. The effective permittivity is displayed in Figure 14. Once again, the aggregate topology exhibits higher effective material parameters, while the deviation increases with increasing particle concentration: there is no difference at the lowest concentration, but for $f = 20\%$ and $f = 30\%$ the deviations are of the same order of magnitude as in the previous case (compare Figures 13 and 14).

4. CONCLUSION

We have performed 3D simulations of loss-free and lossy random binary mixtures on a cubic grid in order to study the transition from aggregate to cermet topology (see Figure 12).

At a low filling factor of $f = 10\%$, where most particles are surrounded by matrix material, no differences in the effective material parameters are observed. At higher concentrations of $f = 20\%$ and $f = 30\%$, both permeability and permittivity vary in a systematic way during the transition. This is an effect of the changing spatial distribution of the particles. Aggregate topology, where the particle positions are random but more restricted, is characterized by the highest effective material parameters. Cermet topology, where arbitrary interparticle distances are possible, exhibits the smallest effective permittivity and permeability values. In this concentration range below the percolation threshold, the concept of topological classes might be of use. Additional simulations are needed in order to quantify the observed effects and to find out whether they persist at smaller dielectric or magnetic contrasts.

ACKNOWLEDGMENT

The authors are grateful to the authors of [9–11] who kindly put their original numerical code at our disposal.

REFERENCES

[1] R. Ramprasad, P. Zurcher, M. Petras, M. Miller, and P. Renaud, "Magnetic properties of metallic ferromagnetic nanoparticle composites," *Journal of Applied Physics*, vol. 96, no. 1, pp. 519–529, 2004.

[2] M. Dikeakos, L. D. Tung, T. Veres, A. Stancu, L. Spinu, and F. Normandin, "Fabrication and characterization of tunable magnetic nanocomposite materials," *Materials Research Society Symposium Proceedings*, vol. 734, pp. 315–320, 2003.

[3] V. B. Bregar, "Advantages of ferromagnetic nanoparticle composites in microwave absorbers," *IEEE Transactions on Magnetics*, vol. 40, no. 3, pp. 1679–1684, 2004.

[4] K. Günther and D. Heinrich, "Dielektrizitätskonstante, Permeabilität, elektrische Leitfähigkeit, Wärmeleitfähigkeit und Diffusionskonstante von Gemischen mit kugelförmigen Teilchen (gitterförmige und statistische Anordnung)," *Zeitschrift für Physik*, vol. 185, no. 4, pp. 345–374, 1965.

[5] D. R. McKenzie, R. C. McPhedran, and G. H. Derrick, "The conductivity of lattices of spheres. II. The body centred and face centred cubic lattices," *Proceedings of the Royal Society of London A*, vol. 362, no. 1709, pp. 211–232, 1978.

[6] L. Fu, P. B. Macedo, and L. Resca, "Analytic approach to the interfacial polarization of heterogeneous systems," *Physyical Review B*, vol. 47, no. 20, pp. 13818–13829, 1993.

[7] N. Harfield, "Conductivity of a periodic particle composite with spheroidal inclusions," *The European Physical Journal—Applied Physics*, vol. 6, no. 1, pp. 13–21, 1999.

[8] N. Harfield, "Bulk permittivity of a composite with coated spheroidal filler particles," *Journal of Materials Science*, vol. 35, no. 23, pp. 5809–5816, 2000.

[9] S. Stölzle, A. Enders, and G. Nimtz, "Numerical simulation of random composite dielectrics," *Journal de Physique I*, vol. 2, no. 4, pp. 401–408, 1992.

[10] S. Stölzle, A. Enders, and G. Nimtz, "Numerical simulation of random composite dielectrics. II. Simulations including dissipation," *Journal de Physique I*, vol. 2, no. 9, pp. 1765–1777, 1992.

[11] H. Leinders and A. Enders, "Computer simulations of dielectric and magnetic composite media including dissipation," *Journal de Physique I*, vol. 5, no. 5, pp. 555–564, 1995.

[12] E. Tuncer and E. Tuncer, "On complex permittivity of dilute random binary dielectric mixtures in two-dimensions," *Turkish Journal of Physics*, vol. 23, pp. 101–105, 2003.

[13] E. Tuncer, B. Nettelblad, and S. M. Gubañski, "Non-debye dielectric relaxation in binary dielectric mixtures (50–50): randomness and regularity in mixture topology," *Journal of Applied Physics*, vol. 92, no. 8, pp. 4612–4624, 2002.

[14] C. Brosseau and A. Beroual, "Computational electromagnetics and the rational design of new dielectric heterostructures," *Progress in Materials Science*, vol. 48, no. 5, pp. 373–456, 2003.

[15] C. Brosseau and A. Beroual, "Dielectric properties of periodic heterostructures: a computational electrostatics approach," *The European Physical Journal—Applied Physics*, vol. 6, no. 1, pp. 23–31, 1999.

[16] V. Myroshnychenko and C. Brosseau, "Finite-element method for calculation of the effective permittivity of random inhomogeneous media," *Physical Review E*, vol. 71, no. 1, Article ID 016701, 16 pages, 2005.

[17] F. Wu and K. W. Whites, "Quasi-static effective permittivity of periodic composites containing complex shaped dielectric particles," *IEEE Transactions on Antennas and Propagation*, vol. 49, no. 8, pp. 1174–1182, 2001.

[18] J. Monecke, "Microstructure dependence of material properties of composites," *Physica Status Solidi (B)*, vol. 154, no. 2, pp. 805–813, 1989.

[19] G. Bánhegyi, "Comparison of electrical mixture rules for composites," *Colloid & Polymer Science*, vol. 264, no. 12, pp. 1030–1050, 1986.

[20] V. M. Shalaev, "Electromagnetic properties of small-particle composites," *Physics Reports*, vol. 272, no. 2-3, pp. 61–137, 1996.

[21] A. Spanoudaki and R. Pelster, "Effective dielectric properties of composite materials: the dependence on the particle size distribution," *Physical Review B*, vol. 64, no. 6, Article ID 064205, 6 pages, 2001.

[22] R. Pelster, "Dielectric spectroscopy of confinement effects in polar materials," *Physical Review B*, vol. 59, no. 14, pp. 9214–9228, 1999.

[23] R. Pelster and U. Simon, "Nanodispersions of conducting particles: preparation, microstructure and dielectric properties," *Colloid and Polymer Science*, vol. 277, no. 1, pp. 2–14, 1999.

[24] S. O. Nelson, "Density-permittivity relationships for powdered and granular materials," *IEEE Transactions on Instrumentation and Measurement*, vol. 54, no. 5, pp. 2033–2040, 2005.

[25] L. K. H. van Beek, "Dielectric behavior of heterogenous systems," in *Progress in Dielectrics*, J. B. Birks, Ed., vol. 7, pp. 69–114, Heywood Books, London, UK, 1967.

[26] S. S. Dukhin, "Dielectric properties of disperse systems," in *Surface Colloid Science*, E. Matijevic, Ed., vol. 3, pp. 83–165, Wiley-Interscience, New York, NY, USA, 1971.

[27] J. D. Jackson, *Classical Electrodynamics*, John Wiley & Sons, New York, NY, USA, 1975.

[28] B. Hallouet, "Simulationen und experimentelle Untersuchungen der dielektrischen und magnetischen Eigenschaften von Nanokompositen," Diploma Thesis, Universität des Saarlandes, Saarbrücken, Germany, 2006.